EXTENDED PDF FORMAT
SPONSORED BY
usb
www.usbweb.com

Science
AAAS

High-Performance Carbon Nanotube Fiber

Krzysztof Koziol, *et al.*

Science **318**, 1892 (2007);
DOI: 10.1126/science.1147635

The following resources related to this article are available online at www.sciencemag.org (this information is current as of January 10, 2008):

Updated information and services, including high-resolution figures, can be found in the online version of this article at:
http://www.sciencemag.org/cgi/content/full/318/5858/1892

Supporting Online Material can be found at:
http://www.sciencemag.org/cgi/content/full/1147635/DC1

This article **cites 19 articles**, 5 of which can be accessed for free:
http://www.sciencemag.org/cgi/content/full/318/5858/1892#otherarticles

This article appears in the following **subject collections**:
Materials Science
http://www.sciencemag.org/cgi/collection/mat_sci

Information about obtaining **reprints** of this article or about obtaining **permission to reproduce this article** in whole or in part can be found at:
http://www.sciencemag.org/about/permissions.dtl

Downloaded from www.sciencemag.org on January 10, 2008

Science (print ISSN 0036-8075; online ISSN 1095-9203) is published weekly, except the last week in December, by the American Association for the Advancement of Science, 1200 New York Avenue NW, Washington, DC 20005. Copyright 2007 by the American Association for the Advancement of Science; all rights reserved. The title *Science* is a registered trademark of AAAS.

2. J. Anandan, *Nature* **360**, 307 (1992).
3. M. V. Berry, *Proc. R. Soc. London Ser. A* **392**, 45 (1984).
4. M. A. Nielsen, I. L. Chuang, *Quantum Computing and Quantum Information* (Cambridge Univ. Press, Cambridge, 2000).
5. J. A. Jones, V. Vedral, A. Ekert, G. Castagnoli, *Nature* **403**, 869 (2000).
6. D. Leibfried *et al.*, *Nature* **422**, 412 (2003).
7. G. Wendin, V. Shumeiko, *Handbook of Theoretical and Computational Nanotechnology*, M. Rieth, W. Schommers, Eds. (American Scientific, Los Angeles, 2006), vol. 3 (www.arxiv.org/abs/cond-mat/0508729v1).
8. M. H. Devoret, A. Wallraff, J. M. Martinis, www.arxiv.org/abs/cond-mat/0411174v1 (2004).
9. T. Yamamoto, Y. A. Pashkin, O. Astafiev, Y. Nakamura, J. S. Tsai, *Nature* **425**, 941 (2003).
10. M. Steffen *et al.*, *Science* **313**, 1423 (2006).
11. A. O. Niskanen *et al.*, *Science* **316**, 723 (2007).
12. J. H. Plantenberg, P. C. de Groot, C. J. P. M. Harmans, J. E. Mooij, *Nature* **447**, 836 (2007).
13. J. Majer *et al.*, *Nature* **449**, 443 (2007).
14. M. A. Sillanpää, J. I. Park, R. W. Simmonds, *Nature* **449**, 438 (2007).
15. G. Falci, R. Fazio, G. M. Palma, J. Siewert, V. Vedral, *Nature* **407**, 355 (2000).
16. X. B. Wang, M. Keiji, *Phys. Rev. B* **65**, 172508 (2002).
17. A. Blais, A. M. S. Tremblay, *Phys. Rev. A* **67**, 012308 (2003).
18. Z. H. Peng, M. J. Zhang, D. N. Zheng, *Phys. Rev. B* **73**, 020502 (2006).
19. M. Mottonen, J. P. Pekola, J. J. Vartiainen, V. Brosco, F. W. J. Hekking, *Phys. Rev. B* **73**, 214523 (2006).
20. Y. Nakamura, Y. A. Pashkin, J. S. Tsai, *Nature* **398**, 786 (1999).
21. A. Shnirman, G. Schön, Z. Hermon, *Phys. Rev. Lett.* **79**, 2371 (1997).
22. V. Bouchiat, D. Vion, P. Joyez, D. Esteve, M. H. Devoret, *Phys. Scr.* **T76**, 165 (1998).
23. D. Vion *et al.*, *Science* **296**, 886 (2002).
24. A. Blais, R. S. Huang, A. Wallraff, S. M. Girvin, R. J. Schoelkopf, *Phys. Rev. A* **69**, 062320 (2004).
25. A. Wallraff *et al.*, *Nature* **431**, 162 (2004).
26. A. Wallraff *et al.*, *Phys. Rev. Lett.* **95**, 060501 (2005).
27. A. Abragam, *Principles of Nuclear Magnetism* (Oxford Univ. Press, Oxford, 1961).
28. Y. Aharonov, J. Anandan, *Phys. Rev. Lett.* **58**, 1593 (1987).
29. G. De Chiara, G. M. Palma, *Phys. Rev. Lett.* **91**, 090404 (2003).
30. G. Ithier *et al.*, *Phys. Rev. B* **72**, 134519 (2005).

31. We thank P. Maurer and L. Steffen for their contributions to the project, and A. Shnirman, J. Blatter, G. De Chiara, and G. M. Palma for valuable discussions. Supported by the EC via an Intra-European Marie Curie Fellowship (P.J.L.), the Natural Sciences and Engineering Research Council of Canada, Canadian Institute for Advanced Research, and Fonds Québécois de la Recherche sur la Nature et les Technologies (A.B.), the National Security Agency under the Army Research Office, NSF, and Yale University (D.I.S., L.F., and R.J.S.), Consiglio Nazionale delle Ricerche–Istituto di Cibernetica, Pozzuoli, Italy (L.F.), the Ontario Research Development Challenge Fund and Mathematics of Information Technology and Complex Systems (J.M.G.), the Swiss National Science Foundation, and ETH Zürich.

29 August 2007; accepted 1 November 2007
Published online 22 November 2007;
10.1126/science.1149858
Include this information when citing this paper.

High-Performance Carbon Nanotube Fiber

Krzysztof Koziol,[1] Juan Vilatela,[1] Anna Moisala,[1] Marcelo Motta,[1] Philip Cunniff,[2] Michael Sennett,[2] Alan Windle[1]*

With their impressive individual properties, carbon nanotubes should form high-performance fibers. We explored the roles of nanotube length and structure, fiber density, and nanotube orientation in achieving optimum mechanical properties. We found that carbon nanotube fiber, spun directly and continuously from gas phase as an aerogel, combines high strength and high stiffness (axial elastic modulus), with an energy to breakage (toughness) considerably greater than that of any commercial high-strength fiber. Different levels of carbon nanotube orientation, fiber density, and mechanical properties can be achieved by drawing the aerogel at various winding rates. The mechanical data obtained demonstrate the considerable potential of carbon nanotube assemblies in the quest for maximal mechanical performance. The statistical aspects of the mechanical data reveal the deleterious effect of defects and indicate strategies for future work.

High-performance synthetic fibers, based on polymer molecules or graphene sheets, have been under development for the past half century, motivated by the high strength and stiffness of the covalent carbon-carbon bond and by the ability to achieve alignment of these bonds with the fiber axis. The key to producing such fibers is to maximize the number of covalently bonded carbon atoms per unit volume or mass, and thus to reduce the proportion of other types of atoms or groups attached to polymer chains. The advantage of pure carbon fibers is that the mechanical properties are derived from the in-plane stiffness and strength of graphene sheets, without the adulterating effect of additional atoms to satisfy available carbon bonds. However, the route to carbon fibers involves the alignment of precursor structures, which are then covalently bonded to each other to create the final structure. This second phase of chemistry not only complicates the processing operation, but also creates a structure in which the basic mechanism that generates toughness in linear polymer systems (i.e., chain pullout) is not available. Carbon fibers are thus comparatively brittle, especially when they are heat-treated to maximize stiffness.

The very high axial strength and stiffness of individual carbon nanotubes, demonstrated both by experiment (*1*–*3*) and modeling (*4*–*6*), opens up the possibility of processing them directly into fibers without the need for a subsequent cross-linking step. Thus, the benefits of high-performance polymeric fibers—especially directness of processing and fiber toughness (measured as energy absorbed up to fracture)—can be combined with the advantages of a fiber consisting only of carbon atoms. If one views carbon nanotubes as extremely strong and stiff polymer molecules, it is not surprising that the processing routes developed so far borrow concepts from polymer fiber–processing technologies. The leading approaches for production of nanotube fibers are (i) spinning from a lyotropic liquid crystalline suspension of nanotubes, in a process similar to that used for polymeric fibers such as aramids (*7*); (ii) spinning from multiwall nanotubes previously grown on a substrate as semi-aligned carpets (*8*, *9*); and (iii) spinning directly from an aerogel of single- and double-walled carbon nanotubes as they are formed in a chemical vapor deposition reactor (*10*). This last process is the one we used (*11*). In terms of mechanical properties, the various techniques have met with different degrees of success. Fibers produced by the liquid crystalline route (*7*) showed an encouraging stiffness of 120 GPa but only modest strengths on the order of 0.1 GPa. Fibers spun from carbon nanotube carpets and subsequently twisted (*9*) have now been made (*12*) with strengths up to 1.9 GPa and stiffnesses up to 330 GPa. An individual strength value of 3.3 GPa was also mentioned (*13*). Until now, the highest strength reported for direct-spun carbon nanotube fiber was 2.2 GPa, and the highest stiffness reported was 160 GPa (*14*).

The mechanical properties of a material are limited by defects within an otherwise perfect structure. In the case of high-performance polymer fibers, these defects consist of chain ends and

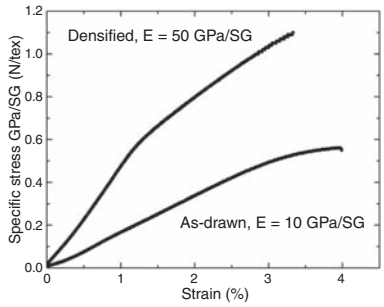

Fig. 1. Specific stress-strain curves for an as-drawn fiber and an acetone-densified fiber. These curves are as-recorded, and the gauge length in each case was 20 mm.

[1]Department of Materials Science, University of Cambridge, Pembroke Street, Cambridge CB2 3QZ, UK. [2]U.S. Army, Natick Soldier Research Development and Engineering Center, 15 Kansas Street, Natick, MA 01760, USA.

*To whom correspondence should be addressed. E-[redacted]

Downloaded from www.sciencemag.org on January 10, 2008

topological defects such as chain entanglements (which prevent perfect alignment and optimum chain packing). Other factors that limit strength are inclusions or voids within the fiber and surface defects, although these are normally eliminated during process development. The first requirement in making high-strength fibers from carbon nanotubes is the availability of nanotubes that are as long and as structurally perfect as possible. Single- or double-walled tubes can be made comparatively free of grown-in defects that lead to kinks, and they also show a tendency to assemble in parallel into bundles. The second step is to align all nanotubes as perfectly as possible with the fiber axis, so as to maximize the translation of their axial properties to those of the fiber. The bonding between adjacent nanotubes is weak in shear (graphite is a lubricant); hence, as great a contact length as possible is necessary to transfer the load into any given nanotube. Another advantage of thin-walled nanotubes (single or double) is that they tend to facet or flatten so as to maximize their contact area. Alignment is typically achieved through mechanical forces, whether applied to a partly linked array of fibers or through fluid-flow forces on a lyotropic suspension. The nanotubes we created are mainly double-walled and of unusually large diameter (4 to 10 nm) and collapse against each other, further enhancing the contact area. They are also on the order of 1 mm long and thus have an axial ratio on the order of 10^5 (*11*).

We describe the results of applying the principles of polymer processing to the direct-spinning method, and we show that exceptional fiber properties can be realized without recourse to fiber twisting (which may detract from ultimate stiffness) or to incorporation of polymers or other agents by subsequent back-diffusion (which will have the same effect). These latter two strategies [suggested by (*9*, *15*)] are, of course, available as post-treatments to the fibers described here. In our process, the act of pulling the aerogel out of the reaction zone axially orients the nanotubes and condenses them into a fiber of low specific gravity (SG), typically 10^{-2} (SG is the density of the material divided by the density of water and is thus a dimensionless parameter). The densification is completed by running the fiber through an acetone vapor stream, which evaporates before the fiber is eventually spooled. A similar, surface tension–based densification phenomenon has been reported on carbon nanotube ribbons (*15*).

The on-line densification process is shown in movie S1 and fig. S1. It is a key processing step, although it does not itself improve carbon nanotube orientation; however, it optimizes the stress transfer between the nanotubes, thus ensuring that the largest proportion of them is fully load-bearing. Figure 1 shows typical stress-strain curves for two fibers: an as-spun fiber in which partial densification has been achieved to give an SG of ~10^{-2}, and a fiber made under exactly the same conditions with an out-of-the-furnace winding rate of 20 m/min but after on-line acetone vapor densification to give an SG of ~1. The strength unit used is specific stress, expressed as GPa/SG, which has exactly the same numerical value as N/tex (tex, a unit widely used in the fiber industry, is the linear density in g/km) (*16*).

Figure 2A shows the effect of fiber winding rate on the orientation of the nanotubes, as measured both by polarized Raman scattering and by small-angle x-ray scattering (SAXS). A basic precept of polymer science is that a higher winding rate results in superior orientation and properties (*17*), and more recently this principle has been shown to apply to carbon nanotubes (*18*). Maximal orientation is particularly desirable in the case of an assembly of carbon nanotubes, as it is crucial to controlling the contact efficiency between the relatively rigid neighboring nanotubes and thus the efficiency of load transfer. The enhancement of densification with improved orientation is shown in Fig. 2B as the effect of winding rate on the SG of the fiber. The plot also shows the decrease in linear density as the fiber is drawn down more at the higher winding rates. The SG values were calculated from measurements of mean fiber diameter and tex, the former ranging from 20 μm at 5.6 m/min to 7 μm at 20 m/min. Figure 2C shows the variation in strength and stiffness of the fibers with changing winding rate, using samples of 2-mm gauge length. The improvement is seen as being principally the result of improved fiber orientation. Although the trends are upward with increasing winding rate and the orientation achieved (orientation parameter = 0.85 from SAXS) should be capable of further improvement, attempts to wind at rates beyond 20 m/min led to increased process difficulty and breakage of the aerogel.

Fibers that were wound at 20 m/min, the optimized condition, were subjected to more extensive mechanical analysis. Figure 3A shows the distribution of specific fiber strengths seen for a range of gauge lengths of fiber with linear density of 0.04 tex. The plot is based on 75 tensile tests. Although the strength distribution for 20-mm gauge lengths peaks close to 1 GPa/SG, at 2-mm and 1-mm gauge lengths the strength distribution becomes bimodal with a second peak at 6.5 GPa/SG, with values in its high tail extending beyond 9 GPa/SG. Such behavior is indicative of "weak points" along the fiber at (random) intervals, at spacings on the same order as the gauge length and much greater than the fiber diameter. The lower-strength peak corresponds to chance occurrence of a defect within the gauge length, and the upper peak to the absence of any such defect. This type of behavior is often recognized at an early stage in the development of any commercial fiber, where the higher-strength peak is sometimes referred to as the "intrinsic strength" (*19*–*23*); in such cases, the challenge of the final elimination of processing defects often is not overcome until the process is scaled up to industrial proportions.

To eliminate variations (on a millimeter scale along the fiber) in the amount of carbon in any cross section of the fiber as an explanation for the apparent high specific strength at short gauge lengths, we used scanning electron microscopy and energy-dispersive x-ray spectroscopy (EDS) to measure the carbon content along lengths of fiber. A typical longitudinal scan for total carbon is shown in fig. S2. It shows a variation of carbon

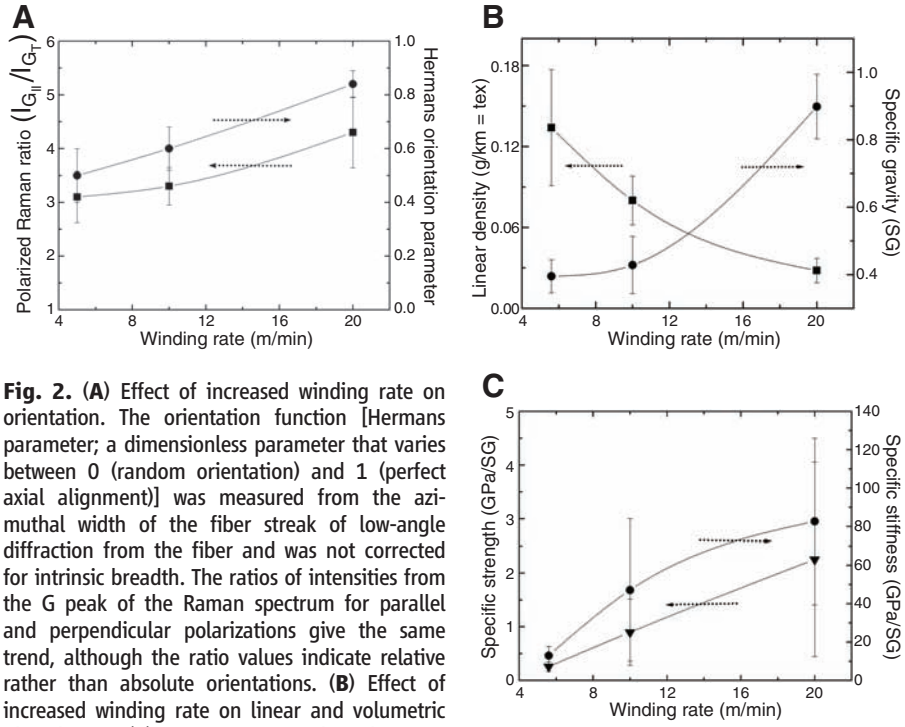

Fig. 2. (**A**) Effect of increased winding rate on orientation. The orientation function [Hermans parameter; a dimensionless parameter that varies between 0 (random orientation) and 1 (perfect axial alignment)] was measured from the azimuthal width of the fiber streak of low-angle diffraction from the fiber and was not corrected for intrinsic breadth. The ratios of intensities from the G peak of the Raman spectrum for parallel and perpendicular polarizations give the same trend, although the ratio values indicate relative rather than absolute orientations. (**B**) Effect of increased winding rate on linear and volumetric fiber density. (**C**) Effect of increased winding rate on average specific strength and average specific stiffness for specimens of 2-mm gauge length.

Downloaded from www.sciencemag.org on January 10, 2008

content along the fiber of between 5 and 7% of the mean. The standard deviation of the diameter was 15.7% of the mean, although we had no guarantee of the fiber roundness, so the cross-sectional area is likely to vary by less than the diameter squared. None of these variations could account for the range of strengths seen in the samples of shorter gauge length. Use of a micro balance to measure the linear density of the samples is quite demanding, as the mass of a sample is on the order of 1 μg and the sensitivity of the balance is on the order of 0.1 μg. The random error associated with these measurements needs to be taken into account; to avoid any risk of exaggerating the strengths reported, we used the highest measurement of linear density (0.04 tex) as the basis for all the strength measurements reported in Figs. 3 and 4.

Figure 3B shows stress-strain curves recorded for three specimens of 1-mm gauge length: one from the lower-strength peak of the distribution, one from the high-strength "intrinsic" peak, and the strongest specimen seen at the upper limit of the distribution. They are compared with a curve for Kevlar 49 measured in our laboratory, which is typical of literature values. An interesting aspect of these curves is that the weaker specimens also show a lower initial modulus. There is also some suggestion of a yield stress, above which the load increases less rapidly with strain, and after which there is not full recovery on unloading before fracture. Figure 3C is a plot of strength versus stiffness, corrected for strain in the grips (a correction that becomes larger for the shortest gauge length, although it was not applied to the nanotube fiber stress-strain curves of Fig. 3B,

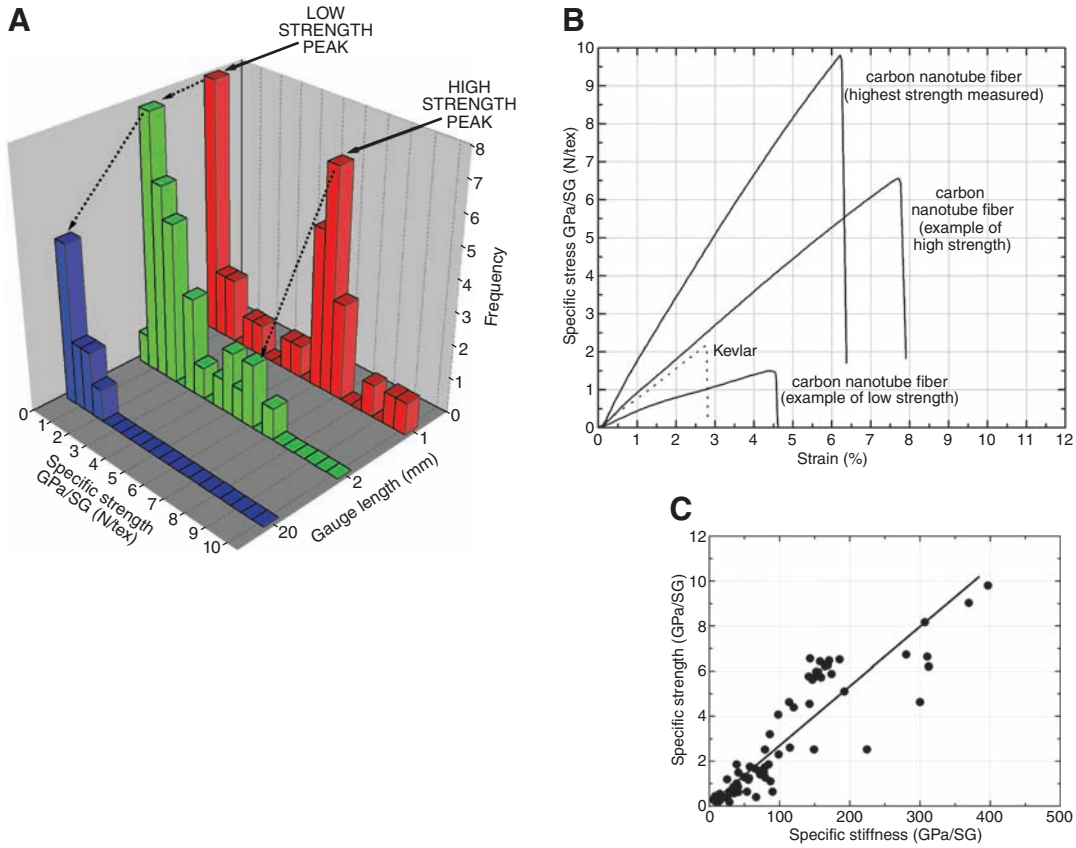

Fig. 3. (**A**) Specific strength distribution of carbon nanotube fibers for different gauge lengths. (**B**) Stress-strain curves for 1-mm specimens for the two strongest carbon nanotube fibers and for fibers typical of the high-strength and low-strength peaks in the distribution. A curve for Kevlar 49 is included as a benchmark. (**C**) Correlation between fiber specific strength and specific stiffness, covering all three gauge lengths. The stiffnesses here are calculated for the low-strain part of the curves with correction for grip strain.

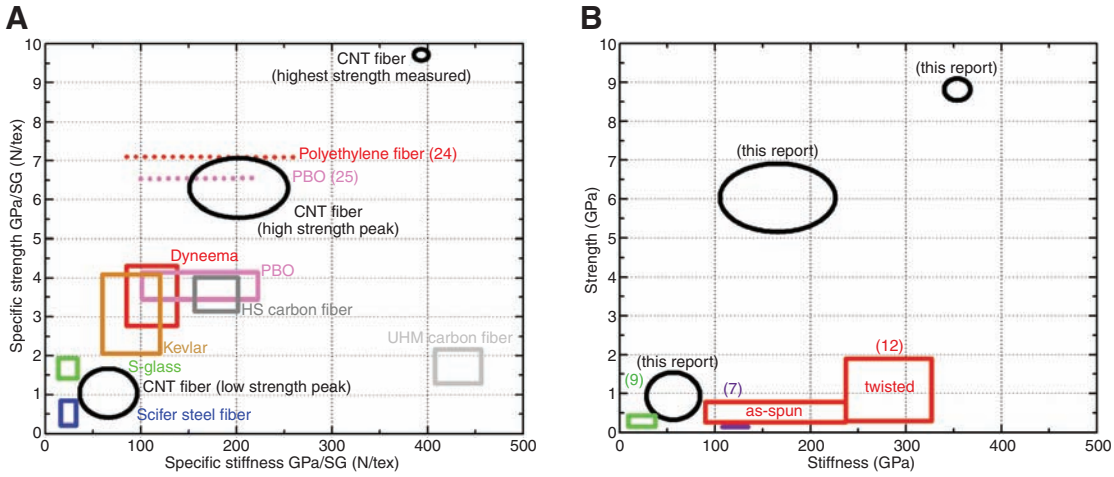

Fig. 4. (**A**) Comparison of the strength and stiffness of our strongest sample and of fibers typical of the high-strength and low-strength peaks in the 1-mm gauge length distribution versus the properties of other commercially available high-performance fibers; two laboratory observations of higher strengths in commercialized systems are also included (reference numbers are shown). (**B**) Similar to (A), but with the strength ranges of our carbon nanotube fibers compared with literature data for other carbon nanotube fibers made by different processes. In this case, the comparison is in terms of GPa instead of GPa/SG. Only data where strength and stiffness values are available from the same samples are included here.

Downloaded from www.sciencemag.org on January 10, 2008

which are as-recorded); this plot reveals a positive correlation between strength and stiffness.

The implication of the correlation between strengths and stiffnesses is that although the fiber samples we created have defects at random intervals on the millimeter scale along the gauge length, these flaws do not have the nature of a stress raiser in a brittle fiber, which would be expected to reduce strength but to have little or no effect on stiffness. It is much more likely that these defects are associated with local deficiencies in densification, which would preclude successful stress transfer by shear between some of the bundles of nanotubes. Consequently, in some sections of the fiber, not all of the nanotube bundles carry an equal share of the load, resulting in both lower fracture strength and decreased stiffness. We believe that these defects are associated with included carbonaceous particles (fig. S3), which induce failure in interbundle stress transfer over much greater distances along the fiber than that occupied by the particle alone. Such particles are seen microscopically with a frequency that is consistent with their distribution at millimeter-scale spacings along the fiber. The strengths reported here represent a measure of success in reducing the level of such included particles, and we expect further levels of process refinement to enable the realization of such high strengths over much longer fibers.

Figure 4A (and table S1) set the strength and stiffnesses of our fibers in the context of a range of mechanical data from commercially available high-performance fibers, as well as reports of properties of other carbon nanotube fibers in the recent literature. The strains shown, and thus the stiffness and energy absorbed up to fracture (table S1), have been corrected for grip strain. Under laboratory conditions, higher strengths than those guaranteed in a commercial product are sometimes seen. Two reported strengths from laboratory fiber work, one for high-strength polyethylene (*24*) and one for poly(*p*-phenylene-2,6-benzobisoxazole) (PBO) (*25*), are plotted as horizontal lines in Fig. 4A. Table S1 also sets the measurements of energy absorbed at fracture (toughness) in the context of other fibers. In Fig. 4B, the performance of our fiber is compared with values reported in the literature for carbon nanotube fibers made by different methods. As some laboratories have not recorded the density of their fibers, we have made this comparison in terms of strength and stiffness rather than specific strength and specific stiffness. One consequence of using these (nonspecific or direct) units is that the estimated error of our measurements is slightly increased.

References and Notes

1. M. F. Yu, B. S. Files, S. Arepalli, R. S. Ruoff, *Phys. Rev. Lett.* **84**, 5552 (2000).
2. M. M. J. Treacy, T. W. Ebbesen, J. M. Gibson, *Nature* **381**, 678 (1996).
3. B. G. Demczyk *et al.*, *Mat. Sci. Eng. A* **334**, 173 (2002).
4. T. Dumitrica, M. Hua, B. I. Yakobson, *Proc. Natl. Acad. Sci. U.S.A.* **103**, 6105 (2006).
5. T. Belytschko, S. P. Xiao, G. C. Schatz, R. S. Ruoff, *Phys. Rev. B* **65**, 235430 (2002).
6. T. Natsuki, K. Tantrakarn, M. Endo, *Carbon* **42**, 39 (2004).
7. L. M. Ericson *et al.*, *Science* **305**, 1447 (2004).
8. K. L. Jiang, Q. Q. Li, S. S. Fan, *Nature* **419**, 801 (2002).
9. M. Zhang, K. R. Atkinson, R. H. Baughman, *Science* **306**, 1358 (2004).
10. Y.-L. Li, I. A. Kinloch, A. H. Windle, *Science* **304**, 276 (2004); published online 11 March 2004 (10.1126/science.1094982).
11. See supporting material on *Science* Online.
12. X. Zhang *et al.*, *Small* **3**, 244 (2007).
13. Q. W. Li *et al.*, *Adv. Mater.* **18**, 3160 (2006).
14. M. Motta, A. Moisala, I. A. Kinloch, A. H. Windle, *Adv. Mater.* **19**, 3721 (2007).
15. B. Vigolo *et al.*, *Science* **290**, 1331 (2000).
16. We express stress as GPa divided by SG, a unit known as specific stress in materials science that is exactly numerically equivalent to newtons per tex.
17. I. M. Ward, Ed., *Structure and Properties of Oriented Polymers* (Halsted/Wiley, New York, 1975).
18. T. Liu, S. Kumar, *Nano Lett.* **3**, 647 (2003).
19. T. Amornsakchai, D. L. M. Cansfield, S. A. Jawad, G. Pollard, I. M. Ward, *J. Mater. Sci.* **28**, 1689 (1993).
20. I. M. Ward, in *Solid Phase Processing of Polymers*, I. M. Ward, P. D. Coates, M. M. Dumoulin, Eds. (Hanser Gardner, Munich, 2000), p. 133.
21. N. Lissart, J. Lamon, *J. Mater. Sci.* **32**, 6107 (1997).
22. R. D. Maurer, Ed., *Strength of Inorganic Glass* (Plenum, New York, 1985).
23. J. D. H. Hughes, H. Morley, E. E. Jackson, *J. Phys. D* **13**, 921 (1980).
24. H. van der Werff, A. J. Pennings, *Colloid Polym. Sci.* **269**, 747 (1991).
25. W. A. Adams, personal communication.

26. Supported by Consejo Nacional de Ciencia y Tecnología (Mexico), the Engineering and Physical Sciences Research Council (UK), and the U.S. Army International Technology Center–Atlantic. We thank S. Fraser for valuable comments and M. Pick for his considerable technical contribution to this research.

Supporting Online Material

www.sciencemag.org/cgi/content/full/1147635/DC1
Materials and Methods
Figs. S1 to S3
Table S1
Movie S1
References

11 July 2007; accepted 2 November 2007
Published online 15 November 2007;
10.1126/science.1147635
Include this information when citing this paper.

Downloaded from www.sciencemag.org on January 10, 2008

Structural Rearrangements That Govern Flow in Colloidal Glasses

Peter Schall,[1,2]* David A. Weitz,[2,3] Frans Spaepen[2]

Structural rearrangements are an essential property of atomic and molecular glasses; they are critical in controlling resistance to flow and are central to the evolution of many properties of glasses, such as their heat capacity and dielectric constant. Despite their importance, these rearrangements cannot directly be visualized in atomic glasses. We used a colloidal glass to obtain direct three-dimensional images of thermally induced structural rearrangements in the presence of an applied shear. We identified localized irreversible shear transformation zones and determined their formation energy and topology. A transformation favored successive ones in its vicinity. Using continuum models, we elucidated the interplay between applied strain and thermal fluctuations that governs the formation of these zones in both colloidal and molecular glasses.

The hallmark of any glass is a very low atomic or molecular mobility within a disordered solid, many orders of magnitude smaller than that of a fluid. This mobility is a result of thermally induced structural rearrangements, which typically occur at a very low rate. Structural rearrangements must also occur as a response of the glass to an externally applied shear; this causes a directional bias in the structural rearrangements that produces the macroscopic strain (*1*). Because the glass structure is so highly constrained, these structural rearrangements must entail reorganization of the constituent molecular units over some larger length scale (*2*). Nevertheless, in molecular glasses, these length scales are still too small and the time scales are too short for direct observation. The only direct evidence for the existence of local shear transformation zones that produce macroscopic strain comes from bubble raft experiments (*3*) and computer simulations of two-dimensional (*4*–*6*) and three-dimensional (3D) glasses (*7*–*10*). Direct real-space visualization of structural rearrangements can be made in suspensions of colloidal particles as they can be quenched into a glassy state by rapid densification of the particles from a fluid state (*11*, *12*). These systems lose ergodicity due to crowding at high particle volume fraction, ϕ, leading to a transition to a glassy state at $\phi_g \approx 0.58$ (*13*). Experiments and simulations suggest that when ϕ_g is approached from the fluid phase, particle rearrangements occur cooperatively on increasing length scales (*2*, *14*, *15*). For $\phi > \phi_g$, such rearrangements are

[1]Van der Waals-Zeeman Institute, University of Amsterdam, Valckenierstraat 65, 1018 XE Amsterdam, Netherlands. [2]Harvard School of Engineering and Applied Sciences, Cambridge, MA 02138, USA. [3]Department of Physics, Harvard University, Cambridge, MA 02138, USA.

*To whom correspondence should be addressed. E-mail: pschall@science.uva.nl